Research Article

Adhesion Dynamics in Probing Micro- and Nanoscale Thin Solid Films

Xiaoling He

School of Material Science and Engineering, Georgia Institute of Technology,
771 Ferst Drive, Atlanta, GA 30332, USA

Correspondence should be addressed to Xiaoling He, xiaoling.he@gatech.edu

This study focuses on modeling the probe dynamics in scratching and indenting thin solid films at micro- and nanoscales. The model identifies bifurcation conditions that define the stick-slip oscillation patterns of the tip. It is found that the local energy fluctuations as a function of the inelastic deformation, defect formation, material properties, and contact parameters determine the oscillation behavior. The transient variation of the localized function makes the response nonlinear at the adhesion junction. By quantifying the relation between the bifurcation parameters and the oscillation behavior, this model gives a realistic representation of the complex adhesion dynamics. Specifically, the model establishes the link between the stick-slip behavior and the inelastic deformation and the local potentials. This model justifies the experimental observations and the molecular dynamics simulation of the adhesion and friction dynamics in both the micro- and nanoscale contact.

1. Introduction

The adhesion and delamination at the interface of micro- and nanoscale thin films are of interest in semiconductor thin films, microstructures, and many other applications. Under stress, defects such as dislocations, twins, and grain boundaries initiate and nucleate. The accumulation of the defects intensifies the local stress field, which eventually induces cracks to release energy. Such a stress and relaxation process continues before the material eventually breaks down at the limit of the adhesive strength of the interfacial material to cause delamination, or at the limit of the coherence strength of the singular material itself that leads to rupture.

An experimental study of the thin film's adhesion property commonly uses a scratching test to determine the adhesion or coherence strength in terms of the critical load with respect to the tip's penetration depth. A diamond stylus scratches the film to generate stresses up to the critical stress intensity till fracture [1, 2]. Experimental observation

indicates that many factors, including material properties and the test conditions, such as the scratching velocity, probing load, and stylus geometry, play a role in the penetration process of the probing tip. Moreover, the tip exhibits oscillatory behavior, in contrast to a direct penetration, subject to the constant driving force or constant driving velocity. This oscillation is generally referred to as the stick-slip behavior in adhesion and friction dynamics, a common phenomenon observed in atomic force microscopy or nanoindentation [3]. The stick-slip behavior is also prevalent in microscale friction dynamics [4]. Savkoor and Briggs also found that during the scratching, a moderate peeling occurs as a result of an increasing shear force. This indicates an irreversible inelastic deformation of the thin film up to fracture. The stick-slip behavior prior to, during, and after the crack initiations suggests highly nonlinear relations between the inelastic deformation, material properties, the forcing, and the contact parameters [5, 6].

Experimental studies have confirmed that interfacial adhesion depends on deformations and accumulating defects such as dislocation, stacking faults, steps, vacancies, pining junctions, and cracks. Studies of adhesion phenomena have taken different perspectives in examining the contact mechanisms at the adhesion junctions. Many of the previous studies have focused on the threshold energy at the initiation of the cracks subjected to different stress fields. The most highlighted theories on adhesion strength are the JKR [7] and DMT models [8, 9]. Both the JKR and DMT models examine the contacting spheres based on Griffith's concept in normal mode fracture. However, a difference exists between the two theories in representing the adhesion forces and the contacting areas. This discrepancy leads to different predicted pull off forces by each theory [10]. Other than these two well-known models, Bradley [11] also evaluated the adhesion threshold strength of two contact bodies by incorporating both the surface energy and the cohesive force based on the Leonard-Jones potential.

For shear-mode fracture, Rice deduced that the stress intensity at the periphery of the contact region is expected to nucleate glide dislocations by an effective Peierls stress [12]. We should mention that Peierls stress refers to a periodic relation between the shear stress and the dislocation-induced sliding at an atomic scale. The Peierls stress arises from the periodicity of the atomic lattice structure. Rice found that the shear stress increases proportionally to the contact size, determined by the unstable stacking fault energy [12]. Hurtado and Kim also developed a model based on a Peierls stress concept [13]. Their model prescribes a slip zone circulating the dislocation region driven by an effective Peierls force.

Until recently, studies on the mixed mode crack, due to a shear force interacting with the normal force in sliding friction, have remained a challenge, both theoretically and experimentally [14]. In addition to the dislocation-induced shear mode crack, which is regarded as the major source of the sliding friction and the initiation of plasticity [12, 13], other defects play a role in the mixed mode fracture, including steps, twins, vacancies, and interstitials [15]. Johnson [10] studied the interaction between the adhesion and friction following Hutchinson's model for joint normal and shear mode fractures [16]. Johnson concluded that the relation between the normal and the shear forces cannot be found by continuum mechanics in a linear model; rather, the response to a combination of normal and tangential forces involves specific characteristics of the nanoscale adhesion junction. The reason is that the nature of this interaction comes from the interface interaction at the periphery of the contact area [10]. Such a mixed mode adhesion or friction problem is typical of the scratching and the nanoindentation of thin solid films using a multifaceted Berkovich tip, shown in Figure 1(a). The driving force pushes the tip into the film as the probe moves forward, which generates both shear and normal forces around the tip. Other configurations

(a) Berkovich tip

(b) Cross-section and overlook of the probe tip

(c) Penetration parameters
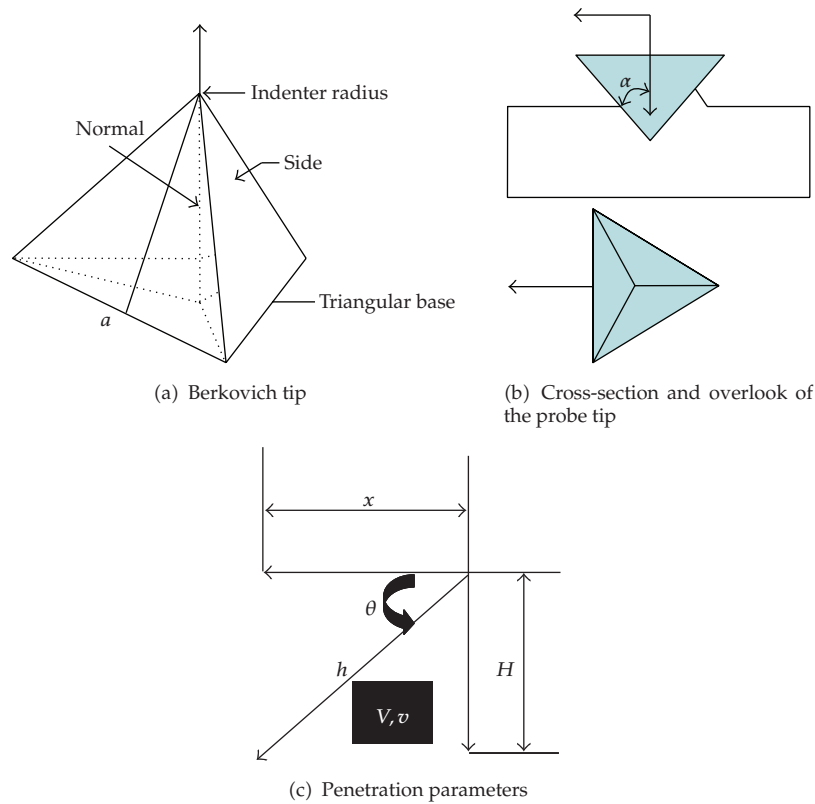
Figure 1: Probe geometry.

of tip profile, such as the parabolic or spherical tips, also give rise to both shear and normal deformation around the tip. The atomic scale molecular dynamics (MD) simulation suggests that the plasticity due to nucleation and the translation of the dislocations is the source of the dynamic stress field around the tip of the indenter, which causes penetration of the tip in a stick-slip behavior [6, 17]. The MD simulation verified the adhesion and friction dynamics at the nanoscale, as observed in experiments. Moreover, both the experiments and the MD computations confirmed that the strain rate-dependent plasticity governs the behavior of nanostructure metals, such as Al and Cu [5, 17].

Different formulations have been used to characterize adhesion and friction dynamics for the stick-slip phenomena of a mechanical system. Persson and Volokitin used a linear vibration model to account for the friction oscillation [4]. The nonlinear model for the friction dynamics by Dankowicz and Nordmark [18] focuses on the chaos and bifurcations in the stick-slip behavior induced by a discontinuous force. The model by Heslot et al. [19] predicts that under a constant driving force, the motion of the contact solids is often unsteady and oscillatory. Both models support the experimental observation of the contact dynamics. These studies analyzed the complexity of the nonlinear behavior in the stick-slip oscillation based on a generalized vibration model. However, these models are not adaptable to explain the stick-slip behavior associated with different deformation mechanisms at the contact interface; in particular, when inelastic deformation is required to account for the strain rate-dependent behavior. Fundamentally, inelastic deformation occurs prior to the crack initiation [20–22].

The underpinning of the inelasticity or plasticity is the irreversible process at the atomic scale due to dislocations and formation of other types of defect, such as twins and grain boundaries [23, 24], which in part, is the cause of the stick-slip oscillation.

It is apparent that the probe dynamics phenomenon of two contacting solids at the adhesion junction should be justified by the deformation mechanisms involved. Although an MD computation can simulate the dynamic behavior of the probe tip, the computation does not prescribe a direct constitutive relation to explain the adhesion dynamics in relation to their deformation mechanisms. On the other hand, the existing formulations for the stick-slip behavior do not incorporate inelastic deformation mechanisms. Therefore, the objective of this study is to develop a model to explain adhesion dynamics associated with both the elastic and inelastic deformations of thin solid films at the micro- and nanoscales. This model builds on Griffith's concept of fracture and inelastic deformation theory for the mixed mode deformation around the probe tip when penetrating thin films subjected to constant driving velocity. By relating the energy release rate to the inelastic deformation of the solid film, we arrive at a relaxation equation to explain the stick-slip behavior in the tip's dynamics at the adhesion junction.

In the following, we will first obtain the equation of motion to describe the dynamics of the probe tip. Further, the stability analysis identifies the bifurcation conditions that define the transitions between a direct sliding penetration mode and a stick-slip relaxation oscillation mode. These bifurcation conditions quantify the dynamics of the tip influenced by a collection of parameters, determined by the local energy function, the contact parameters, and the inelastic material properties for both micro- and nanoscale thin films. Subsequently, the computation illustrates the tip's dynamics in either a direct penetration or a stick-slip behavior. Finally, the paper concludes with a discussion of the adhesion dynamics with respect to the underlying physics of the deformable solids, and the scale effect.

2. Equation of motion

We assume that a probe approaches the thin film at a constant driving velocity V, as shown in Figure 1(c). The probe penetrates the material with both normal and tangential forces at the contacting surfaces, while the multifaceted probe keeps the angle θ close to 10 degrees. Denoting v as the actual velocity of the tip along the penetration direction, $\dot{\varepsilon}$ the strain rate of the thin film, V the driving velocity of the probe, and h the displacement of the tip, the relation between these parameters is

$$V = v + h\dot{\varepsilon}, \tag{2.1}$$

where $\varepsilon = \delta h/h$ is the strain of the thin film along the probe direction, and $v = \dot{h}$ is the actual velocity of the penetration. The relation (2.1) comes from the derivative of the total travel distance L of the tip, which is given by

$$L = h + h\varepsilon. \tag{2.2}$$

This relation holds when the probe traverses through the atomic lattice and displaces the atoms for dislocations at the nanoscale, or when the penetration induces inelastic deformation in the creeping of the microscale thin films. Along with the penetration, defects migrate and accumulate to produce a high stress field to slow down the tip's motion, whereas the probe

overcomes the energy barrier to proceed. This process repeats until the incipient of cracks, which gives the energy release rate per unit contact area as

$$G_c = \phi(v) + \varphi(v) + I(\dot{v}).$$ (2.3)

Here $\phi(v)$ is the inelastic energy loss near the crack tip, which is proportional to the surface energy, $\varphi(v)$ is the inelastic energy loss away from the crack tip, and $I(\dot{v})$ is the inertia energy. Since the far-field energy release $\varphi(v)$ is negligible due to the localized deformation surrounding the tip, the energy release rate simplifies to

$$G_c = \phi(v) + I(\dot{v}).$$ (2.4)

The equivalent mass associated with the inertia in the unit contact length is

$$m = \frac{I(\dot{v})}{d\dot{v}}.$$ (2.5)

This leads to

$$\frac{dG_c}{dt} = m\ddot{v} + \dot{v}\frac{d(\phi(v))}{dv}.$$ (2.6)

On the other hand, the strain energy release balances against the increase in the surface energy [14], which means

$$G_c = \sigma h + \tau\Omega = \sigma h(1 + \eta) = \tilde{\sigma}h.$$ (2.7)

Here σ and τ are the normal stress and shear stress, respectively; $\tilde{\sigma}$ represents the combined stress of a joint normal and shear stress field, Ω stands for the total surface area of the activation volume of the contact plane, and $\eta = \tau\Omega/\sigma h$ is the shear factor. This factor is an indicator for the major deformation in either shear or normal mode, which makes the oscillation represent either the friction or the adhesion dynamics, respectively. The derivative of the energy release rate with respect to time gives

$$\dot{G}_c = \frac{dG_c}{dt} = \frac{\partial(\tilde{\sigma}h)}{\partial t} = (\dot{\tilde{\sigma}} + \tilde{\sigma}\dot{\varepsilon})h.$$ (2.8)

This suggests that the energy release rate of the inelastic deformation depends on the time-dependent strain rate. In reference to the theory of time-dependent plasticity in solids by Persson [15], the mean stress filed σ with respect to the mean strain field ε and the strain rate $\dot{\varepsilon}$ can be described by the relation of

$$E\dot{\varepsilon} = \dot{\sigma} + \tilde{\lambda}(t)\sigma.$$ (2.9)

Here E is Young's modulus; $\tilde{\lambda}(t)$ and $\eta(t)$ are parameters associated with the deformation mechanisms and material properties, and they are related by $\tilde{\lambda}(t) = E/\eta(t)$. The solution to (2.9) as a first-order ordinary differential equation is in the general form of

$$\sigma(t) = \frac{E}{\mu(t)} \left[\int_0^t \mu(t)\varepsilon(t)dt + \sigma_0 \right], \quad \mu(t) = e^{\int_0^t \tilde{\lambda}t} = e^{\lambda t}. \tag{2.10a}$$

This can be further approximated in a series expression, as:

$$\sigma(t) = \frac{E}{\lambda}\dot{\varepsilon}(t) - \left(\frac{E}{\lambda^2}\right)\ddot{\varepsilon}(t) + \cdots (-1)^{n+1}\left(\frac{E}{\lambda^n}\right)\varepsilon^{(n)} + \sigma_0, \quad \varepsilon^{(n)} = \frac{d^{(n)}\varepsilon}{dt^{(n)}}. \tag{2.10b}$$

After dropping the higher-order strain-rate, we obtain

$$\tilde{\sigma} \cong A_0\varepsilon + B_0\dot{\varepsilon} - C_0\ddot{\varepsilon}, \quad A_0 = E, \; B_0 = \frac{E}{\lambda}, \; C_0 = \frac{E}{\lambda^2}, \tag{2.11}$$

where $\sigma_0 = E\varepsilon$ represents the yield stress at the limit of elastic deformation; $B_0\dot{\varepsilon}$ and $C_0\ddot{\varepsilon}$ result from the inelastic deformation that is strain rate-dependent. To justify the negative strain effect, that is, the strain softening along with a plastic flow when the tip passes through a trail of voiding, or the strain hardening due to a high energy barrier while experiencing a reduced deformation, the coefficient λ, or effectively B_0, can be negative. A positive coefficient B_0 stands for an increasing deformation along with an intensified stress field. Both coefficients B_0 and C_0 can be regarded as time-dependent localized functions determined by defect formations, localized energy functions, material properties, and contact parameters, such as the activation volume or contact length.

Ignoring the second-order strain terms, the time derivative of the energy release rate becomes

$$\dot{G}_c = \dot{\tilde{\sigma}}h = \left(A\dot{\varepsilon} + B\ddot{\varepsilon} - C\dddot{\varepsilon}\right)h, \tag{2.12a}$$

where all coefficients can be time-dependent functions and given by

$$A = E + \dot{B}_0, \qquad B = B_0 - \dot{C}_0, \qquad C = C_0. \tag{2.12b}$$

From the velocity analysis, the time-dependent strain rate is related to the velocity by

$$\dot{\varepsilon} = \frac{V - v}{h}, \tag{2.13}$$

which yields

$$\ddot{\varepsilon} = -\frac{(V - v)v}{h^2} - \frac{\dot{v}}{h}. \tag{2.14}$$

Since $(V - v) \ll v$, we have

$$\ddot{\varepsilon} \approx -\frac{\dot{v}}{h}, \qquad \dddot{\varepsilon} = -\frac{\ddot{v}}{h}. \tag{2.15}$$

Using (2.12a) and (2.12b), we obtain

$$\begin{aligned}
\frac{d\tilde{\sigma}}{dt} &= A\dot{\varepsilon} + B\ddot{\varepsilon} - C\dddot{\varepsilon} \\
&= A\left(\frac{V - v}{h}\right) + B\left(-\frac{\dot{v}}{h}\right) + C\frac{\ddot{v}}{h}.
\end{aligned} \tag{2.16}$$

Equations (2.16) and (2.6) lead to

$$\dot{v}\frac{d\phi}{dv} + m\ddot{v} = \left[A(V - v) - B\dot{v} + C\ddot{v}\right], \tag{2.17}$$

which is equivalent to

$$\ddot{v} + \mu\omega\left(\frac{d\phi}{dv} + B\right)\dot{v} + \omega^2(v - V) = 0, \tag{2.18a}$$

where

$$\omega^2 = \frac{A}{\tilde{m}}, \quad \mu = \frac{1}{\tilde{m}\omega} = \sqrt{\frac{1}{\tilde{m}A}}, \quad \tilde{m} = m - C. \tag{2.18b}$$

This is Leonard's equation in a typical relaxation oscillation that describes the jerky motion of the probing dynamics. The parameters in this equation quantify the influence of the elastic and inelastic deformation moduli, contacting parameters, and the driving velocity on the probing dynamics. The equation indicates that the oscillation frequency is determined by both the elastic and inelastic deformation moduli and the mass contained in the activation volume, that is,

$$\omega^2 = \frac{E + \dot{B}}{\rho\Omega - C}. \tag{2.19}$$

The unit mass $m = \rho\Omega$ is related to the inertia energy release by (2.5). The forcing of this jerky motion is

$$\frac{dF}{dt} = \omega^2 V = \frac{(E + \dot{B})V}{\rho\Omega}. \tag{2.20}$$

Equation (2.20) indicates that an intensified forcing comes from a reduced contact area or a smaller volume of mass, and from the high elasticity, a time-dependent variation of inelastic

modulus and a high driving velocity. Another term in (2.18a) is $\mu\omega(d\phi/dv + B)$, which represents the friction damping in the probing process. The antidamping coefficient μ is defined as

$$\mu = \frac{1}{\tilde{m}\omega} = \sqrt{\frac{1}{\tilde{m}(E + \dot{B})}} = \sqrt{\frac{1}{\rho(E + \dot{B})\Omega}} > 0. \tag{2.21}$$

Under constant driving velocity, it is natural to assume that the inelastic energy dissipation at the interface is a function of the driving velocity and the local energy release. Introducing the function $\chi(\phi) = d\phi/dv$, (2.18a) becomes

$$\ddot{v} + \mu\omega(\chi(\phi) + B)\dot{v} + \omega^2(v - V) = 0. \tag{2.22}$$

$\chi(\phi)$ measures the inelastic energy release rate at the tip with respect to the penetration rate. This function can be a time-dependent function during the penetration, even though the driving velocity is constant. In conjunction with the inelastic deformation modulus B, $(\chi(\phi)+B)$ reflects the localized energy dissipation or energy accumulation rate, influenced by the local energy barriers, and the inelastic deformation mechanisms at different length scales. For example, dislocation at the atomic level requires energy that is several orders less than that for creeping at the microscale. On the other hand, the contact parameters could also differ by the same order between the two length scales. Such combinations could produce a product in $\mu(\chi(\phi) + B)$ that is the same for the two different length scales to prescribe similar oscillation behavior of the tip, as analyzed below.

Note that the energy release rate for cracks or defect formation implies that

$$\frac{d\phi}{dv} = \chi(\phi) > 0. \tag{2.23}$$

This is because the energy release function $\phi(v) > 0$ symbolizes an energy loss at the tip, and $\phi(v) < 0$ an energy gain due to an intensified stress field. Therefore, the motion at $\phi(v) < 0$ has a reduced penetration rate due to an increasing energy barrier, that is, $v < 0$ and $\phi(v) = \chi(\phi)v < 0$. On the other hand, $\phi(v) > 0$ corresponds to an increasing penetration rate at $v > 0$ with energy dissipation, and $\phi(v) = \chi(\phi)v > 0$.

3. Stability analysis

The bifurcation conditions determine the oscillation patterns and their stabilities. In matrix form, (2.22) becomes

$$\left\{ \begin{array}{c} \dot{u} \\ \dot{v} \end{array} \right\} = \begin{bmatrix} -\mu\omega(\chi(\phi) + B) & -\omega^2 \\ 1 & 0 \end{bmatrix} \left\{ \begin{array}{c} u \\ v \end{array} \right\} + \left\{ \begin{array}{c} \omega^2 V \\ 0 \end{array} \right\}, \tag{3.1}$$

where $u = \dot{v}$ is the acceleration. The eigenvalues of this linear system are

$$\lambda_{1,2} = \frac{\omega}{2}\left(-\mu(\chi(\phi) + B) \pm \sqrt{\mu^2(\chi(\phi) + B)^2 - 4} \right). \tag{3.2}$$

The eigenvalues indicate that there are several oscillation patterns in the phase diagram, which are determined by the collective parameter $\mu\omega(\chi(\phi) + B)$ [25]. It is apparent that both the elastic and the inelastic deformation rate influence the oscillation stability or the bifurcation behavior, as analyzed below.

(a) $(\chi(\phi) + B) = 0$, $\lambda_{1,2} = \pm i\omega$, periodic oscillation

This is the condition for the Hopf bifurcation. The velocity is periodic, given as

$$\ddot{v} + \omega^2 v = \omega^2 V. \tag{3.3}$$

The condition $\chi(\phi) + B = 0$ indicates a balance between the inelastic energy release rate and an inelastic deformation energy variation in a negative strain effect, $B < 0$. This occurs when the tip goes through vacancies to cause the reduced stress intensity due to strain softening, while discharging energy along with the penetration. Alternatively, a higher energy barrier develops at a reduced deformation at $B < 0$ for strain hardening when accumulated defects prevent the tip from further penetrating the film. When $\chi(\phi) + B = 0$, there is insufficient energy to stop the motion completely by the high energy barrier, or to sustain a continuous penetration. Instead, a cyclic velocity occurs, alternating between $v > 0$ and $v < 0$, respectively. This corresponds to two phases of negative strain fields, that is, the strain softening and hardening, which give rise to the stick-slip oscillation.

(b) $(\chi(\phi) + B) > 0$, $\mathrm{Re}(\lambda_{1,2}) < 0$, stable oscillations

From (3.2), if $\mu(\chi(\phi) + B) \geq 2$, there are two real negative eigenvalues. The oscillation converges to a stable node in the phase diagram, reaching the driving velocity after a transient oscillation. This allows for a continuous penetration with energy release through deformation or crack. If $0 < \mu(\chi(\phi) + B) < 2$, the complex conjugate eigenvalues, $\lambda_{1,2} = \mathrm{Re}(\lambda_{1,2}) \pm i\,\mathrm{Im}(\lambda_{1,2})$ with a negative real part, define the subcritical Hopf bifurcation, in which the penetration velocity oscillates in a spiral pattern to the nodal velocity at V. The spiral motion is the consequence of two alternating stress field: that is, the intensified stress field due to the strain hardening, and a reduced stress field associated with a moderate creeping or voiding. In this case, the penetration is partially constrained by energy barriers from strain hardening effect.

(c) $(\chi(\phi) + B) < 0$, $\mathrm{Re}(\lambda_{1,2}) > 0$, unstable oscillations

If $\mu(\chi(\phi) + B) \leq -2$, two positive real eigenvalues make an unstable nodal oscillation. On the other hand, if $0 > \mu(\chi(\phi) + B) > -2$, then $\lambda_{1,2} = \mathrm{Re}(\lambda_{1,2}) \pm i\,\mathrm{Im}(\lambda_{1,2})$ defines a supercritical Hopf bifurcation in an unstable spiral motion. In both cases, there is a dominant negative strain effect to make $(\chi(\phi) + B) < 0$ due to the strain softening. The velocity keeps increasing deviating from the driving velocity due to the predominant creeping or voiding, which results in a straight forward penetration. A spiral oscillatory velocity occurs when the creeping is intertwined with the intermittent energy barriers or energy releases through cracks.

The bifurcation conditions indicate that the oscillation pattern is determined mainly by the parameter $(\chi(\phi) + B)$ associated with the local energy barriers and inelastic deformation. The fluctuation of the collective parameter in the form $\mu(\chi(\phi) + B)$ gives rise to transitions

(a) Velocity-acceleration phase diagram

(b) Stick-slip penetration
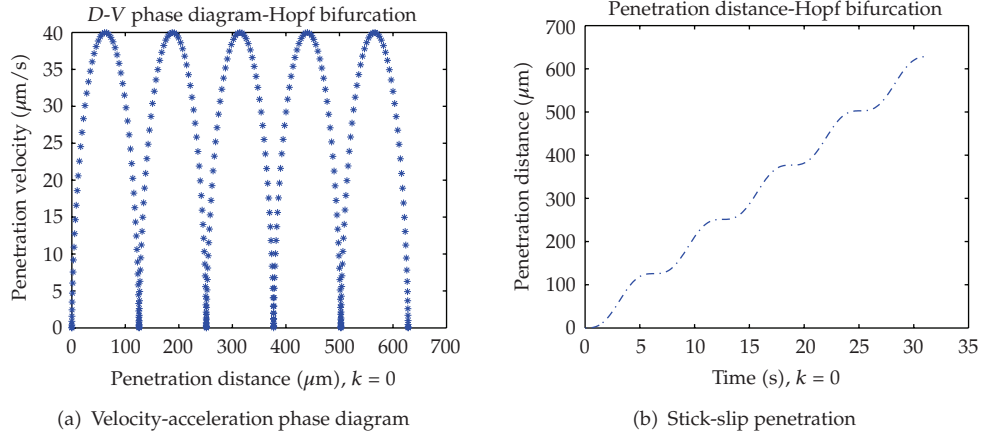
Figure 2: Periodic oscillation.

among different bifurcations. The antidamping coefficient μ influences such transitions by variable contact area and material properties.

4. Numerical computation

The computation is based on the normalized equation (2.22) using the time scale $\tau = \omega t$, which yields

$$\frac{d^2v}{d\tau^2} + \mu(\chi(\phi) + B)\frac{dv}{d\tau} + (v - V) = 0. \tag{4.1}$$

The time step is $\Delta\tau = 0.1\,\text{s}$ using the 4th-order Runge-Kutta method. The bifurcation condition is specified in the form of $\mu(\chi(\phi) + B) = 2k$, where k is a constant chosen for each case. Using different values of μ and $(\chi(\phi) + B)$ for the contact, deformation, and the energy release rate at different length scales of the Cu thin film, the numerical results below illustrate the oscillatory patterns determined by the above bifurcation conditions for contact at both micro- and nanoscales.

4.1. Microscale thin film behavior

We choose $E = 105\,[\text{GPa}]$, $G = 42\,[\text{GPa}]$ for the microscale Cu thin film, the same as the bulk material properties. We also set B a constant, or $\dot{B} = 0$. The density of the Cu film is $\rho = 8.9\,[\text{g/cm}^3]$. The driving velocity is $V = 20\,[\mu\text{m/s}]$. The contact area is $A_c = 22.67h_0^2\,[\mu\text{m}^2]$ at a fixed contact length of $h_0 = 0.4\,[\mu\text{m}]$. Figure 2(a) shows the periodic oscillation of the velocity with respect to the travel distance for the bifurcation case 1: $(\chi(\phi) + B) = 0$. The velocity-distance phase diagram traces back to the ellipsoid phase portrait for the acceleration and velocity represented by (3.3). Figure 2(b) is the periodic penetration depth with respect to time in a stick-slip oscillation, which shows a repeated forward and an almost standstill motion due to a cyclic velocity variation. The penetration in a forward motion traverses a distance about $100\,\mu\text{m}$ in each stroke. As already explained, such a periodic behavior indicates a penetration cycle where the creeping deformation alternates

(a) Velocity-acceleration phase diagram in the subcritical Hopf bifurcation at $k = 0.5$

(b) Penetration distance in a subcritical Hopf bifurcation at $k = 0.5$

(c) Velocity-acceleration phase diagram in a stable node at $k = 3$

(d) Penetration distance in a stable node at $k = 3$
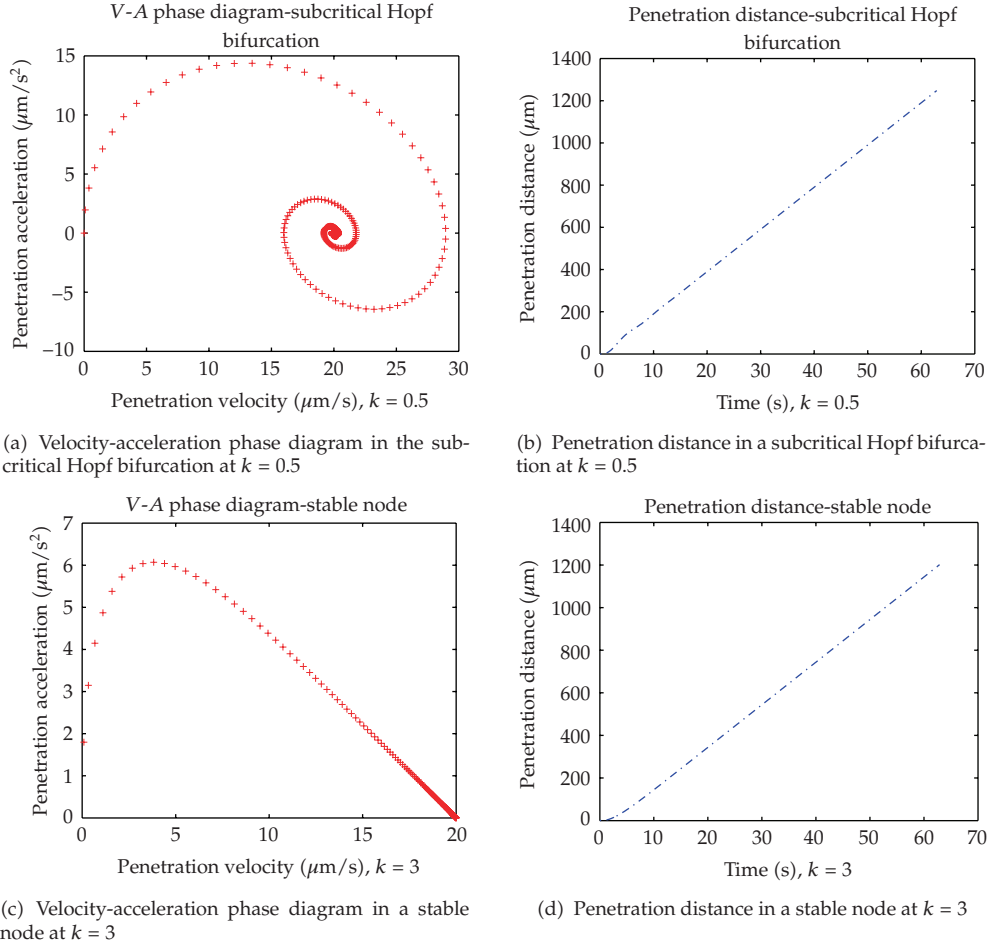
Figure 3: Stable oscillation for $\mu(\chi(V) + B) > 0$.

with the strain hardening motion due to the defect-induced energy barriers. The higher energy barrier pushes the tip to nearly a standstill before the external energy overcomes the barrier to move the tip forward again.

For the bifurcation case 2: $(\chi(\phi) + B) > 0$. Figures 3(a) and 3(b) illustrate the oscillation in a stable spiral pattern, whereas Figures 3(c) and 3(d) are in a stable nodal pattern, respectively. For the stable spiral oscillation, the parameters are set as $\mu(\chi(\phi) + B) = 6$ at $k = 3$, while the stable node oscillation corresponds to $\mu(\chi(\phi) + B) = 1$ at $k = 0.5$. The velocity approaches the node in both phase diagrams, reaching $v = V = 20\,[\mu\text{m/s}]$. Notably, the stable oscillation in either a spiral pattern or a nodal pattern makes the tip traverse in a direct penetration at the driving velocity at the steady state. A slight difference exists in the penetration rate between these two cases, as shown in Figures 3(c) and 3(d), respectively, owing to different transient oscillations.

For case 3: $\mu(\chi(\phi) + B) < 0$. Figures 4(a) and 4(b) illustrate the unstable spiral motion while Figures 4(c) and 4(d) are for the unstable nodal pattern. The unstable spiral is subjected to $\mu(\chi(\phi) + B) = -1$ for $k = -0.5$, while the unstable node corresponds to $\mu(\chi(\phi) + B) = -4$ at $k = -2$. Both unstable oscillations make the velocity increases continuously. The spiral

(a) Penetration distance-velocity phase diagram in the supercritical Hopf bifurcation at $k = -0.5$

(b) Penetration distance in a supercritical Hopf bifurcation at $k = -0.5$

(c) Penetration distance-velocity phase diagram in an unstable node at $k = -2$

(d) Penetration distance in an unstable node at $k = -2$
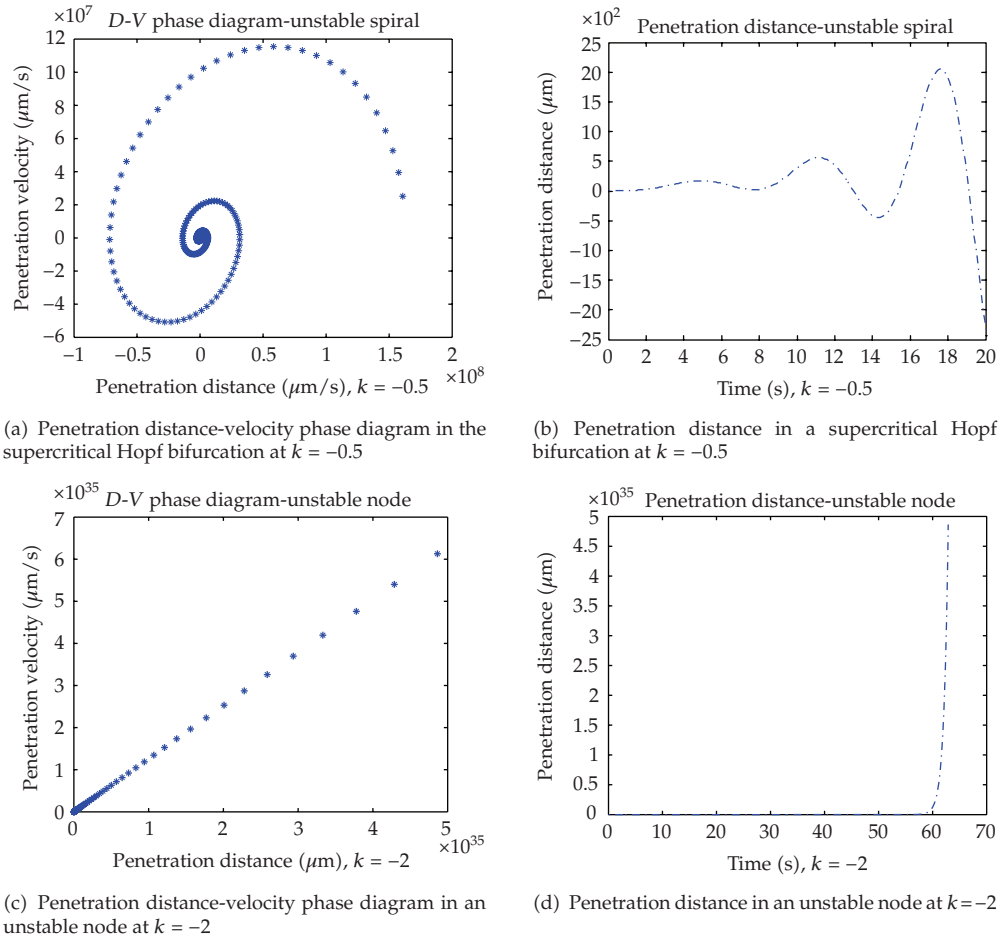
Figure 4: Unstable oscillation for $\mu(\chi(V) + B) < 0$.

velocity introduces a backward and forward stick-slip behavior, as shown in Figure 4(b). On the other hand, the unstable nodal pattern enables a direct penetration shown in Figure 4(d). Note that nodal-type unstable penetration may not occur in reality, the unlimited creeping is unlikely to occur to produce an unstable nodal type penetration, due to defects that induce energy barriers to effectively constrain tip's motion.

4.2. The influence of periodic potentials

The above results confirm that the tip's penetration behavior is determined by the deformation mechanisms that are reflected by the bifurcation conditions. As illustrated in both Figures 2(b) and 4(b), the stick-slip behavior occurs when the velocity is in either a periodic oscillation or an unstable spiral motion, corresponding to the Hopf bifurcation or the supercritical Hopf bifurcation, respectively. The stick-slip penetration could also be a manifestation of the continuous transitions among different bifurcations due to the variable bifurcation parameters. This could occur because the localized defects and deformation introduce instantaneous changes of the local potentials, contact areas, and energy release rate.

(a) Penetration distance-velocity diagram at a periodic potential at $k = 2$ and $j = 3$

(b) Penetration distance at a periodic potential $k = 2$ and $j = 3$

(c) Penetration distance-velocity diagram at a periodic potential $k = 1$ and $j = 3$

(d) Penetration distance at a periodic potential $k = 1$ and $j = 3$
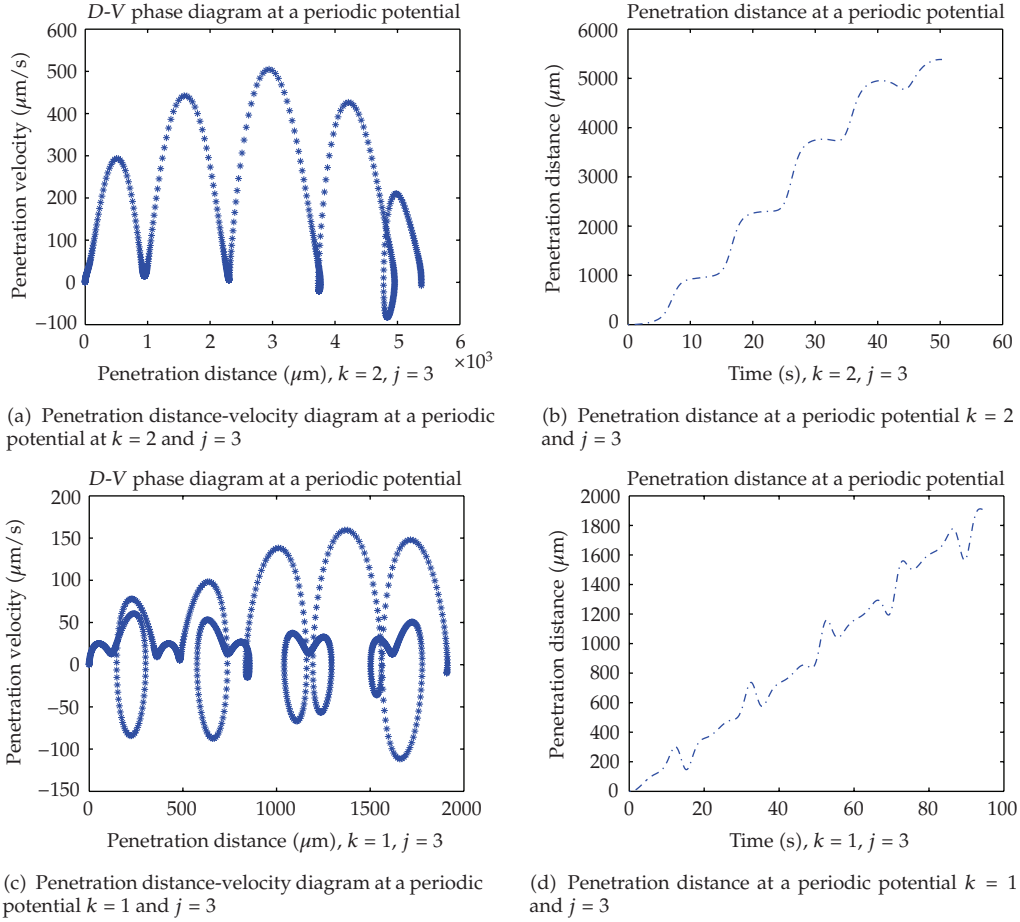
Figure 5: Nonperiodic oscillations subject to a periodic potential $\mu(\chi(V) + B)\cos(k\tau/j)$.

To simulate the influence of a periodic variation of the local potentials associated with the energy release rate, the collective bifurcation parameter is set in a time-dependent trigonometric function, that is, $\mu(\chi(\phi) + B)\cos(k\tau/j) = 2k\cos(k\tau/j)$. Figures 5(a) and 5(b) show the stick-slip behavior corresponding to the potential function at $k = 2$ and $j = 3$, which leads to $\mu(\chi(\phi) + B)\cos(k\tau/j)$ oscillating periodically within $[-4, 4]$. The phase diagram in Figure 5(a) shows a nonperiodic velocity that is almost all positive, which makes the stick-slip penetration in a forward-standstill pattern, as shown in Figure 5(b). The penetration behavior is due to the instantaneous transitions among all five bifurcations described above in each cycle. By varying the parameters, for example, $k = 1$ and $j = 3$, identical bifurcation transitions take place, since the range of $\mu(\chi(\phi) + B)\cos(k\tau/j)$ is $[-2, 2]$. Here three types of the Hopf bifurcations dominate, that is, the oscillation transits mainly among the stable spiral, unstable spiral, and periodic oscillations. However, both the backward and forward stick-slip motion are present in each cycle due to the velocity alternating between positive and negative values, as shown in Figures 5(c) and 5(d). Each stroke of the slip motion traverses a different distance. These results demonstrate that a periodic energy barrier leads to a quasiperiodic stick-slip oscillation owing to transitional bifurcations. Effectively, the periodic energy release

and inelastic deformation transform the system into a nonlinear relaxation model. As a result, the oscillation is no longer in a fixed frequency in each cycle; instead, a variable frequency oscillation occurs.

The influence of the periodic bifurcation parameters in another form, that is, $\mu(\chi(\phi) + B\cos(k\tau/j))$, a periodic inelastic deformation that goes along with a constant energy release rate $\chi(\phi)$, indicates that an unstable oscillation prevails when the transitional bifurcation parameter $\mu(\chi(\phi) + B\cos(k\tau/j)) < 0$. For example, an unstable spiral for $\mu(\chi(\phi) + B\cos(k\tau/j)) = -4 + 2\cos(k\tau/j) < 0$ generates a stick-slip oscillation, similar to that shown in Figure 4(b). On the contrary, a stable oscillation emerges to give rise to a forward penetration when $\mu(\chi(\phi) + B\cos(k\tau/j)) = 2 + 2\cos(k\tau/j) = [4, 0]$.

The difference in the forms of the periodic potential affects both the transient and the steady-state oscillation behavior. Physically, these periodic variations can be attributed to different material behavior and factors at the adhesion junction, including the contact area, the elastic and inelastic deformation moduli, the energy dissipation and the external forcing, among others. Note that periodic potential variation directly reflects the atomic potentials of crystals in a periodic structure that gives rise to Peierls stress in shear mode deformation, which constitutes the energy barrier for sliding dislocations.

We should also point out that a variable contact area contributes to the dynamic variation of the bifurcation conditions. This is because the depth of the penetration influences the contact area, which indirectly affects the parameter μ and the bifurcation condition $\mu(\chi(\phi) + B)$. During the probing, the tip remains in contact with the solid film until the crack debris peels off from the thin film, upon which the contact length may reduce to zero, or to a critical length. This is because cracks counterbalance the increasing activation volume or the contact length around the tip. The critical contact length defines the transition upon which the penetration process repeats itself. Therefore, the contact area variation can be regarded as a source of the periodic or an irregular variation of local energy release rate. The wider range variations of the local energy potentials can lead to complex dynamics in the tip's oscillation, compared to that under the periodic potentials. This also means that the real tip's nonlinear stick-slip behavior becomes more complex, due to the instantaneous fluctuation of the contact parameters and energy functions.

4.3. Contact dynamics at the nanoscale

As has been shown, the computation results phenomenologically agree with the experimental observation of the stick-slip or the direct penetration behavior in the microscale thin films. By examining (4.1) it is apparent that an identical relaxation behavior exists with the nanoscale thin films at a different energy level. This is because the collective parameter $\mu(\chi(\phi) + B)$ defines the oscillation behavior, even though different energy function $(\chi(\phi) + B)$ and contact parameter μ are specified. This makes the model adaptable to describe both the micro- and the nanoscale phenomena. In fact, the model in (2.22) agrees with the dislocation dynamics equation that accounts for the dislocation displacement fluctuation at the atomic lattice when overcoming a finite mass at the pining junction, as described by Osip'yan and Vardanian in [26].

To illustrate the tip dynamics when penetrating a nanoscale thin film, we use a periodic potential in the form $\mu(\chi(\phi)\cos(k\tau/j) + B)$, for the periodic energy releases accompanied by a constant inelastic deformation module $B > 0$. Figures 6(a)–6(d) compare the transition of the penetration behaviors for a fixed contact area and a continuously variable contact area. The bifurcation parameters vary in the range $\mu\chi(\phi)(\cos(k\tau/j) - 2) = [18, 6]$ with

(a) Velocity-acceleration phase diagram at a constant contact area

(b) Slip penetration at a constant contact area

(c) Velocity-acceleration phase diagram at a variable contact area

(d) Stick-slip penetration at a variable contact area
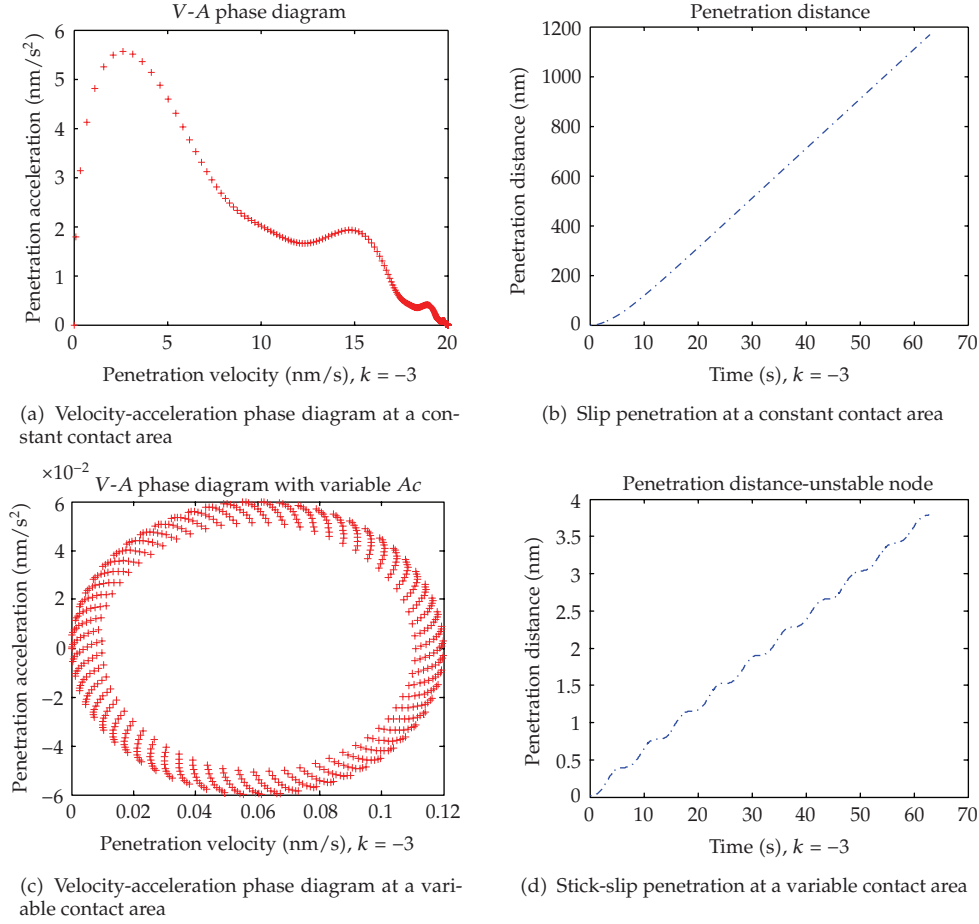
Figure 6: Nanoscale oscillations with $\mu\chi(V)(\cos(k\tau/j) - 2)$, $\mu\chi(V) = 2k$, $k = -3$, and $j = 3$.

$\mu\chi(\phi) = 2k$, $k = -3$, $j = 3$. For the fixed contact area with a contact length of $h_0 = 0.4$ nm, the condition defines a stable oscillation approaching a constant nodal velocity at the steady state, as shown in Figure 6(a), giving rise to a direct penetration as displayed in Figure 6(b). However, an increasing contact area of the form $A_c = \alpha h^2$ transforms the nodal-type velocity and acceleration phase diagram into a quasiperiodic oscillation pattern, as shown in Figure 6(c). This indicates the effective transitions of the bifurcation parameters due to a decreasing antidamping coefficient μ as a result of an increasing contact area. The velocity oscillates in a positive but declining range and the penetration is in a forward-standstill type stick-slip behavior, as shown in Figure 6(d). At a driving velocity of $V = 0.06$ nm/s, the stick-slip oscillation reveals that each stroke is of the order of the atomic lattice parameter $a = 0.364$ nm for Cu. This suggests that dislocations occur at the Berger's vector length, since the Berger's vector $|\vec{b}| = a$ for a perfect dislocation [27].

For the Cu nanoscale thin film interacting with the tip, the above computation used the ideal shear strength $\tau_{\max} = 2.5$ GPa [28, 29], which renders the dislocation line energy $E_b = 2$ eV/nm, based on $E_b = G\vec{b}^2$ for a perfect dislocation [27]. This energy level agrees with established results for a dislocation and void initiation, which is generally in the order

of E_b = 5 eV per Berger's vector [30]. The MD simulation of the Cu void growth and dislocation process indicates that the activation energy is E_b = 2.3~3.5 eV/nm [31]. Note that the dislocation energy through dissociation is found to be $E_d = 1.3~2.7$ eV from a higher to lower temperature range [32]. The dislocation nucleation and parallel formation require an energy level that is less than that for a perfect dislocation, as confirmed by the MD simulation [5, 6]. Similarly, twins and the stacking faults formed along with the dislocation nucleation, all of which are activated at a reduced energy level compared to that for a perfect dislocation. Therefore, the stick-slip behavior indicates the onset of plasticity due to dislocations and other defects, including vacancies, twins, stacking faults, and so forth. Alternatively, it can be said that the stick-slip oscillation is a reflection of the process whereby defects initiate and nucleate to induce a periodic or an arbitrary fluctuation of the energy release rate at the atomic scale due the tip's probe of the thin film.

5. Discussion

(1) The present study discusses a model that distinguishes the scale effect by local energy functions, namely, the inelastic deformation and energy dissipation, as well as contact parameters at the adhesion junction. The localized energy function at the microscale is associated with the creep due to strain rate-dependent inelastic deformation and cracks, while the energy function at the nanoscale is due to the dislocation-induced plasticity and nucleation of other defects. The local contact parameter, energy fluctuations, and inelastic deformation at the adhesion interface define a collective bifurcation parameter to describe the stick-slip behavior at both micro- and nanoscales. Although each parameter can be explicitly specified, it is the collective parameter $\mu(\chi(\phi) + B)$ that defines the stick-slip behavior.

(2) This model bridges the inelastic deformation mechanism and local energy release with the tip's oscillation patterns. By incorporating a variable energy release along with the inelastic deformation, this model reveals that the variations of the potential, the inelastic deformation modulus, or the contact parameters, in a periodic or an arbitrary manner, are the underlying mechanisms of the nonlinear stick-slip behavior. The transitional bifurcation behavior justified the underpinning physics of adhesion dynamics. By relating the stick-slip behavior of the tip to thin film's deformation mechanisms, interfacial energy release, defects, contact parameters, material properties, and forcing conditions at the peripheral of the contact, this model brings the analytical prediction closer to the experimental observation of the stick-slip phenomena.

(3) The stick-slip oscillation at both the nanoscale and microscale suggests that the Griffith concept for the energy release at the crack tip is adaptable to describing the onset of plasticity by dislocation migration and nucleation at the nanoscale. Furthermore, the periodic bifurcation condition adopted in the computation represents the typical energy fluctuation at the atomic scale, since it is consistent with the Peierls stress concept associated with the sliding dislocations of the atomic lattice. Such variations also represent the energy barrier at the microscale deformation influenced by the cyclic contact parameters and repeated energy release through cracks. In addition to the adaptability of the model to the tip's dynamics at both micro- and nanoscale, the model allows for an arbitrary energy fluctuation for complex interfacial contact behaviors.

(4) Although this model describes the adhesion dynamics in a scratching process, the stress field and the tip oscillation behavior are identical to the friction dynamics observed in the nanoindentation, when a higher shear factor characterizes the motion [6]. This is because the friction force in the nanoindentation involves deformations in both normal and shear

modes. Essentially, this model is capable of describing the nonlinear dynamics at the tip-solid interface of both the friction and adhesion dynamics.

6. Conclusion

This work develops a model to describe the adhesion and friction dynamics at the interface of two contacting solids for the tip and thin solid film interaction, such as those during an AFM adhesion microscopy or nanoindentation process. The bifurcation conditions generated from this model give a proper account of the interplay between the localized energy functions, the elastic and inelastic deformations, the material properties, and the contact parameters that collectively influence the tip's dynamics at the adhesion junction. The bifurcation conditions attribute the stick-slip behavior of the tip to the Hopf bifurcations and the transitional bifurcations associated with a periodic or an arbitrary potential variation, defect formations, and inelastic deformations at the contact interface. The model reveals that these interactive parameters give rise to the nonlinear oscillation in penetration patterns. The collective parameters determine the adhesion and friction dynamics at the periphery of the contact of both micro- and nanoscales.

References

[1] P. A. Steinmann, Y. Tardy, and H. E. Hintermann, "Adhesion testing by the scratch test method: the influence of intrinsic and extrinsic parameters on the critical load," *Thin Solid Films*, vol. 154, no. 1-2, pp. 333–349, 1987.

[2] J. Ye, N. Kojima, K. Ueoka, J. Shimanuki, T. Nasuno, and S. Ogawa, "Nanoscratch evaluation of adhesion and cohesion in SiC/low-k/Si stacked layers," *Journal of Applied Physics*, vol. 95, no. 7, pp. 3704–3710, 2004.

[3] A. R. Savkoor and G. A. D. Briggs, "The effect of a tangential force on the contact of elastic solids in adhesion," *Proceedings of the Royal Society A*, vol. 356, no. 1684, pp. 103–114, 1977.

[4] B. N. J. Persson and A. J. Volokitin, *Sliding Friction: Physical Principles and Application*, Springer, New York, NY, USA, 1997.

[5] T. Zhu, J. Li, A. Samanta, H. G. Kim, and S. Suresh, "Interfacial plasticity governs strain rate sensitivity and ductility in nanostructured metals," *Proceedings of the National Academy of Sciences of the United States of America*, vol. 104, no. 9, pp. 3031–3036, 2007.

[6] K. J. Van Vliet, J. Li, T. Zhu, S. Yip, and S. Suresh, "Quantifying the early stages of plasticity through nanoscale experiments and simulations," *Physical Review B*, vol. 67, no. 10, Article ID 104105, 15 pages, 2003.

[7] K. L. Johnson, K. Kendall, and A. D. Roberts, "Surface energy and the contact of elastic solids," *Proceedings of the Royal Society A*, vol. 324, no. 1558, pp. 301–313, 1971.

[8] B. V. Derjaguin, V. M. Muller, and Yu. P. Toporov, "Effect of contact deformations on the adhesion of particles," *Journal of Colloid and Interface Science*, vol. 53, no. 2, pp. 314–326, 1975.

[9] B. V. Derjaguin, V. M. Muller, and Yu. P. Toporov, "On the role of molecular forces in contact deformations (critical remarks concerning Dr. Tabor's report)," *Journal of Colloid and Interface Science*, vol. 67, no. 2, pp. 378–379, 1978.

[10] K. L. Johnson, "Continuum mechanics modeling of adhesion and friction," *Langmuir*, vol. 12, no. 19, pp. 4510–4513, 1996.

[11] R. S. Bradley, "The cohesive force between the solids and the surface energy of the solids," *Philosophical Magazine*, vol. 13, pp. 853–862, 1932.

[12] J. R. Rice, "Dislocation nucleation from a crack tip: an analysis based on the Peierls concept," *Journal of the Mechanics and Physics of Solids*, vol. 40, no. 2, pp. 239–271, 1992.

[13] J. A. Hurtado and K.-S. Kim, "Scale effects in friction of single-asperity contacts—I: from concurrent slip to single-dislocation-assisted slip," *Proceedings of the Royal Society A*, vol. 455, no. 1989, pp. 3363–3384, 1999.

[14] K. L. Johnson, "Adhesion and friction between a smooth elastic spherical asperity and a plane surface," *Proceedings of the Royal Society A*, vol. 453, no. 1956, pp. 163–179, 1997.

[15] B. N. J. Persson, "Theory of time-dependent plastic deformation in disordered solids," *Physical Review B*, vol. 61, no. 9, pp. 5949–5966, 2000.

[16] J. W. Hutchinson, "Mixed mode fracture mechanics of interfaces," in *Metal and Ceramic interfaces*, M. Rühle, A. G. Evans, A. M. Ashby, and J. P. Hirth, Eds., pp. 295–306, Pergamon Press, New York, NY, USA, 1990.

[17] J. Li, K. J. Van Vliet, T. Zhu, S. Yip, and S. Suresh, "Atomistic mechanisms governing elastic limit and incipient plasticity in crystals," *Nature*, vol. 418, no. 6895, pp. 307–310, 2002.

[18] H. Dankowicz and A. B. Nordmark, "On the origin and bifurcations of stick-slip oscillations," *Physica D*, vol. 136, no. 3-4, pp. 280–302, 2000.

[19] F. Heslot, T. Baumberger, B. Perrin, B. Caroli, and C. Caroli, "Creep, stick-slip, and dry-friction dynamics: experiments and a heuristic model," *Physical Review E*, vol. 49, no. 6, pp. 4973–4988, 1994.

[20] B. N. J. Persson, "Time-dependent plastic deformation in solids," in *Sliding Friction*, pp. 382–393, Springer, Berlin, Germany, 2000.

[21] W. Yan, E. P. Busso, and N. P. O'Dowo, "A micromechanics investigation of sliding wear in coated components," *Proceedings of the Royal Society A*, vol. 456, no. 2002, pp. 2387–2407, 2000.

[22] N. B. Jayaweera, J. R. Downes, M. D. Frogley, et al., "The onset of plasticity in nanoscale contact loading," *Proceedings of the Royal Society A*, vol. 459, no. 2036, pp. 2049–2068, 2003.

[23] J.-J. Kim, Y. Choi, S. Suresh, and A. S. Argon, "Nanocrystallization during nanoindentation of a bulk amorphous metal alloy at room temperature," *Science*, vol. 295, no. 5555, pp. 654–657, 2002.

[24] W. D. Nix and H. Gao, "Indentation size effects in crystalline materials: a law for strain gradient plasticity," *Journal of the Mechanics and Physics of Solids*, vol. 46, no. 3, pp. 411–425, 1998.

[25] S. H. Strogatz, *Nonlinear Dynamics and Chaos: With Applications to Physics, Biology, Chemistry and Engineering*, Perseus Books, Cambridge, Mass, USA, 2000.

[26] Y. A. Osip'yan and R. A. Vardanian, "Dynamics of dislocations in the field of point obstacles," in *Crystal Lattice Defects and Dislocation Dynamics*, R. A. Vardanian, Ed., pp. 149–187, Nova Scientific, New York, NY, USA, 2000.

[27] D. Hull and D. J. Bacon, *Introduction to Dislocations*, Butterworth-Heinemann, Oxford, UK, 2001.

[28] D. Roundy, C. R. Krenn, M. L. Cohen, and J. W. Morris Jr., "Ideal shear strengths of fcc aluminum and copper," *Physical Review Letters*, vol. 82, no. 13, pp. 2713–2716, 1999.

[29] S. Ogata, J. Li, and S. Yip, "Ideal pure shear strength of aluminum and copper," *Science*, vol. 298, no. 5594, pp. 807–811, 2002.

[30] H. Föll, 2007, http://www.tf.uni-kiel.de/matwis/amat/def_en/index.html.

[31] M. R. Gungor, D. Maroudas, and S. Zhou, "Molecular-dynamics study of the mechanism and kinetics of void growth in ductile metallic thin films," *Applied Physics Letters*, vol. 77, no. 3, pp. 343–345, 2000.

[32] A. G. Tweet, "Precipitation of Cu in Ge," *Physical Review*, vol. 106, no. 2, pp. 221–224, 1957.